Journal of Thermal Analysis and Calorimetry (2019) 135:2655–2663
https://doi.org/10.1007/s10973-018-7447-9

Folding thermodynamics of PET-hydrolyzing enzyme Cut190 depending on Ca^{2+} concentration

Satomi Inaba[1,2] · Narutoshi Kamiya[3,4] · Gert-Jan Bekker[3] · Fusako Kawai[5] · Masayuki Oda[1]

Received: 6 February 2018 / Accepted: 27 May 2018 / Published online: 4 June 2018

Abstract

The enzyme, cutinase from *Saccharomonospora viridis* AHK190 (Cut190), can hydrolyze the inner block of polyethylene terephthalate (PET). Cut190 has a unique feature that both its activity and thermal stability are increased upon Ca^{2+} binding. In consideration of the glass transition temperature of PET, which is between 60 and 65 °C, the increased activity and thermal stability are of great interest to apply for PET bio-recycling. Our previous mutational analysis showed that the S226P/R228S mutant (Cut190*) has a higher activity and thermal stability than those of the wild type. In this study, we analyzed the folding thermodynamics of the inactive mutant of Cut190*, Cut190*S176A, using circular dichroism and differential scanning calorimetry. The results show that the denaturation temperature increases from 54 to 71 °C due to the addition of 250 mM Ca^{2+}, in a Ca^{2+} concentration-dependent manner. The increased thermal stability is mainly due to the increased enthalpy change, partially compensated by the increased entropy change. Based on the crystal structure of Cut190*S176A bound to Ca^{2+}, molecular dynamics simulations were carried out to analyze the effects of Ca^{2+} on the structural dynamics, showing that the Ca^{2+}-bound structure fluctuated less than the Ca^{2+}-free structure. Structural analysis indicates that Ca^{2+} binding increases the intramolecular interactions of the enzyme, while decreasing its fluctuation, which are in good correlation with the experimental results of the folding thermodynamics.

Keywords Circular dichroism · DSC · Molecular dynamics simulations · Protein conformational change

Introduction

Cutinases (EC 3.1.1.74) belong to a lipase superfamily and were found to catalyze the hydrolysis of complex plant biopolymers in the cuticle layer of leaves (cutin), as well as in the suberin layer of roots (suberin), when cutinases were discovered as a tool of phytopathogenic fungi to invade into the plant surfaces [1, 2]. Because cutinases hydrolyze various substrates such as lipids, waxes, and synthetic esters, as well as catalyzing esterification and transesterification reactions and are produced by fungi, bacteria, and plant pollen [3], they have been used as biocatalysts in industrial applications for the synthesis and bioconversion of chemical compounds [4, 5]. Degradation of polyethylene terephthalate (PET) is of increasing interest as plastic disposal attracts worldwide attention and enzymatic hydrolysis of PET has been evaluated for this purpose [6, 7]. It is noteworthy that surface hydrolysis of PET films or fibers has been observed by serine hydrolases even at temperatures lower than the glass transition temperature

✉ Masayuki Oda
oda@kpu.ac.jp

1 Graduate School of Life and Environmental Sciences, Kyoto Prefectural University, 1-5 Hangi-cho, Shimogamo, Sakyo-ku, Kyoto 606-8522, Japan

2 Research and Utilization Division, Japan Synchrotron Radiation Research Institute, 1-1-1 Kouto, Sayo, Hyogo 679-5198, Japan

3 Institute for Protein Research, Osaka University, 3-2 Yamadaoka, Suita, Osaka 565-0871, Japan

4 Graduate School of Simulation Studies, University of Hyogo, 7-1-28 Minatojima Minami-machi, Chuo-ku, Kobe, Hyogo 650-0047, Japan

5 Center for Fiber and Textile Science, Kyoto Institute of Technology, Matsugasaki, Sakyo-Ku, Kyoto 606-8585, Japan

(T_g) of PET (which is between 60 and 65 °C in aqueous solution), although significant decay of the polymer structure (especially the inner block leading to significant mass loss) was only detected at temperatures higher than T_g [6, 8]. This is due to the increased mobility of the polymer chain at temperatures higher than T_g, making the approach of an enzyme cleaving the polymer body feasible, although the enzyme has to be thermostable at least at temperatures around T_g. In addition, PET hydrolases have to possess a larger active center that can accommodate an aromatic ring, compared with aliphatic polyester hydrolases. Because of limitations with respect to the substrate specificity and thermostability required for PET hydrolysis, there are still only a few examples of cutinases able to significantly hydrolyze the inner block of PET [8].

We previously cloned a few cutinases from thermophilic actinomycetes, *T. alba* AHK119 and *Saccharomonospora viridis* AHK190 [8–10]. Our structural and functional analysis, together with mutational analysis, revealed that a mutant of cutinase from *Saccharomonospora viridis* AHK190 (Cut190), S226P/R228S, denoted as Cut190*, was the best enzyme for PET degradation given its activity and thermal stability [8]. The enzyme Cut190 has a unique feature that Ca^{2+} binding increases both the activity and the thermal stability [8], which resulted in an increase in hydrolysis of two PET films by 14 and 27% at 63 °C. Because the PET-hydrolyzing activity increases with increasing temperatures, high thermal stability of Ca^{2+} bound Cut190* is of interest for both basic science of protein chemistry and industrial applications. Our previous crystal structure analysis of the Cut190 mutant S226P has shown that a Ca^{2+} ion is coordinated within a loop which induces large conformational changes in three loops corresponding to the β1–β2 loop, the β3–α2 loop, and the β4–α3 loop [11]. Furthermore, recent crystal structure analysis of an inactive mutant, Cut190*S176A, in complex with Ca^{2+} and a substrate has shown that three Ca^{2+} ions bind to the protein surface (Fig. 1), one of which is the same site reported previously [11], and regulate the catalysis.

In this study, to understand the molecular mechanism of increased stability induced upon Ca^{2+} binding, we analyzed the folding thermodynamics of Cut190*S176A under various concentrations of Ca^{2+}, using circular dichroism (CD) and differential scanning calorimetry (DSC). We also analyzed the effects of Ca^{2+} binding on the structural dynamics of Cut190*S176A using molecular dynamics (MD) simulations on both the Ca^{2+}-bound and Ca^{2+}-free structures under various Ca^{2+} concentrations starting from the corresponding crystal structures. The thermodynamic origin of the increased stability could be explained by the conformational change in Cut190*S176A induced upon Ca^{2+} binding.

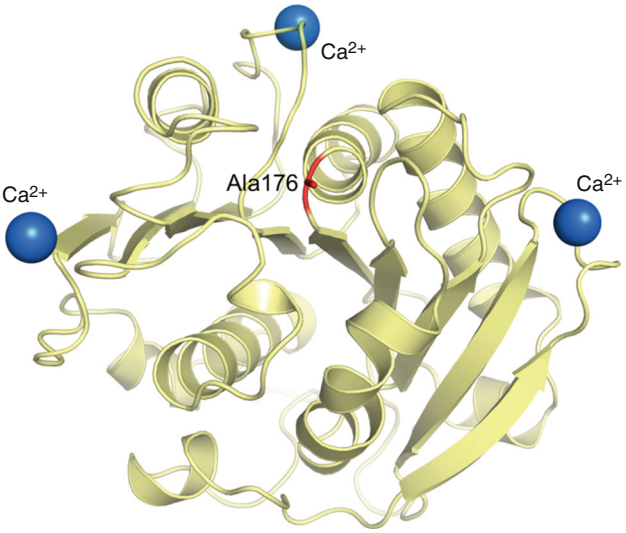

Fig. 1 The crystal structure of Cut190*S176A in complex with Ca^{2+} (PDB ID; 5zno). The blue spheres indicate Ca^{2+} molecules

Experimental

Preparation of Cut190*S176A

The expression plasmid of pQE80L-cut190*S176A was used for transformation of *E. coli* Rosetta-gami B (DE3) cells, as described previously [8]. The protein was expressed under a M9 minimum medium [12], in order to obtain the Ca^{2+}-free sample. The harvested cells were suspended in 20 mM Tris–HCl buffer (pH 8.0) containing 500 mM NaCl and 20 mM imidazole and were disrupted by sonication at 4 °C. After the cell debris was removed by centrifugation, the supernatant was applied to a Ni–NTA column (Qiagen) and the protein was eluted by 200 mM imidazole. The fractions containing the enzyme were pooled and the buffer was exchanged with 10 mM Tris–HCl (pH 8.0). After digestion of the His-tag using the Turbo-3C precision protease (Accelagen), the protein solution was loaded into a MonoQ Sepharose column (GE Healthcare) and eluted using a linear gradient of NaCl with the AKTA purifier system (GE Healthcare). Finally, the buffer was exchanged with 10 mM Tris–HCl (pH 8.0) and the protein concentrations were determined using a UV absorption coefficient at 280 nm of 4.02×10^4 M^{-1} cm^{-1}.

CD measurements

The far-UV CD melting curves were recorded on a J-820 spectropolarimeter (JASCO). The measurements were taken for 0.04 mg mL^{-1} protein in 10 mM Tris–HCl (pH 8.0) containing 0, 0.25, 2.5, 25, or 250 mM $CaCl_2$, using a quartz cell with a 1.0 cm path length. The melting curves were recorded in variable temperature mode at 222 nm,

from 20 to 75, 80, or 85 °C with a heating rate of 1.0 °C min^{-1}. The analysis of the transition curves obtained by temperature-scanning CD measurements was performed on the basis of a two-state transition model, as described previously [13, 14]. The curve fitting was carried out by the nonlinear least-squares method using the OriginPro 2017 software.

DSC measurements

DSC experiments were carried out on a VP-capillary DSC (Malvern Panalytical). The data were collected by heating the solution from 5 to 90 °C at a rate of 1 °C min^{-1}. The sample was reheated without exchanging the solution in the cells to check the reversibility. The outer buffer solution recovered from the final dialysis experiment was used in the reference cell for each case. The protein concentrations were at 1.0 mg mL^{-1} in 10 mM Tris–HCl (pH 8.0) containing 0, 2.5, 25, or 250 mM $CaCl_2$. The data were analyzed using the Origin 7.0 software supplied by the manufacturer, and the fitting analysis was performed using the Origin 5.0 software. The ΔC_p was calculated from the difference in the C_p values between the unfolded and folded states at the denaturation temperature (T_d). The calorimetric enthalpy change (ΔH_{cal}) was calculated by integrating the area in each heat capacity curve, as described previously [13, 14].

MD simulations

Two structures of Cut190*S176A with and without Ca^{2+} were built based on the Ca^{2+}-bound structure (PDB ID; 5zno, Fig. 1) and on the Ca^{2+}-free one (PDB ID; 4wfi). The Ca^{2+}-bound structure has two chains, A and B. Here, chain B was chosen, because this chain was determined with a longer sequence than chain A. Ser176 in the 4wfi structure (Ca^{2+}-free structure) was mutated to Ala by removing the Oγ atom. In addition, Arg228 was mutated to Ser by changing the side-chain atoms, resulting in both the Ca^{2+}-bound and the Ca^{2+}-free structures having the same amino acid sequence. To simulate Ca^{2+} dependence, four computational systems of 0, 25, 100, and 250 mM $CaCl_2$ solutions were constructed for each Cut190*S176A conformation. Here, 0, 7, 21, and 47 Ca^{2+} ions were soaked into the systems of 0, 25, 100, and 250 mM $CaCl_2$, respectively, and the total charge was neutralized by adding chloride ions. For the Ca^{2+}-bound structure, the locations of the initial Ca^{2+} ions were kept when soaking the ions into the systems, while the newly added ions (all ions in the case of the Ca^{2+}-free system) were placed randomly in the solvent of the simulation box. All of the charged residues (Asp, Glu, Arg, and Lys) were treated in their charged forms. Only for the systems of 0 mM $CaCl_2$, five sodium ions were soaked to neutralize them. Explicit water molecules were placed around the protein with a margin of 0.9 nm using a truncated dodecahedron box, with an edge length of ∼ 7.43 nm. The force field parameters for the protein and water molecule were Amber ff99SB-ILDN [15] and TIP3P [16], respectively, and those of the monovalent and divalent ions were based on previous reports [17, 18].

Gromacs 2016.4 was used to prepare the systems and perform the MD simulations with a time step of 2 fs [19]. Electrostatic interactions were treated by the zero-dipole summation method [21], which performs fast calculations at high accuracy comparable to the particle mesh Ewald method [22]. The zero-dipole method has been applied to MD simulations of various systems [20, 23–27]. After energy minimization, ten parallel simulations were executed with each a different random seed for the initial velocities of the atoms to improve the statistics for each system. Here, first NVT (100 ps at 300 K) and NPT (100 ps at 1 bar and 300 K) equilibration simulations were executed on each of the seeds, followed by a 100-ps NVT simulation at 300 K, with position restraints applied on the solute heavy atoms during the equilibration simulations. Finally, productive runs, which amount to 8 μs of simulation in total (= 100 ns × 10 parallel simulations × 2 structures × 4 Ca^{2+} concentrations), were executed. The structure trajectories were stored at every 10 ps. To analyze the trajectories, the Q value, which corresponds to the atomic contact fraction with respect to each initial structure, was calculated. Here, the Q value is equal to 1 when all of the contacts are conserved and is to 0 when they are completely broken. The Q value was averaged from 30 to 100 ns over all parallel trajectories in each system. Furthermore, the Ca^{2+}-bound system at various calcium concentrations was further analyzed by their root mean square deviation (RMSD) and by using principal component analysis (PCA).

Results

Thermal transitions of purified Cut190*S176A in the absence or presence of Ca^{2+} were monitored by measuring the intensity change in the CD values at 222 nm. The apparent fractions in the unfolded states were plotted as a function of temperature (Fig. 2a). The crystal structure analysis shows that the S226P mutant of Cut190 has a 35.9% α-helical and a 21.2% β-sheet structure (Fig. 1), which would reflect the process of thermal unfolding for the overall structures. The thermal unfolding was irreversible, and the CD values in the denatured state under high $CaCl_2$ concentration were close to 0. The results indicate that the protein forms aggregation after thermal denaturation, and most of them would be precipitated,

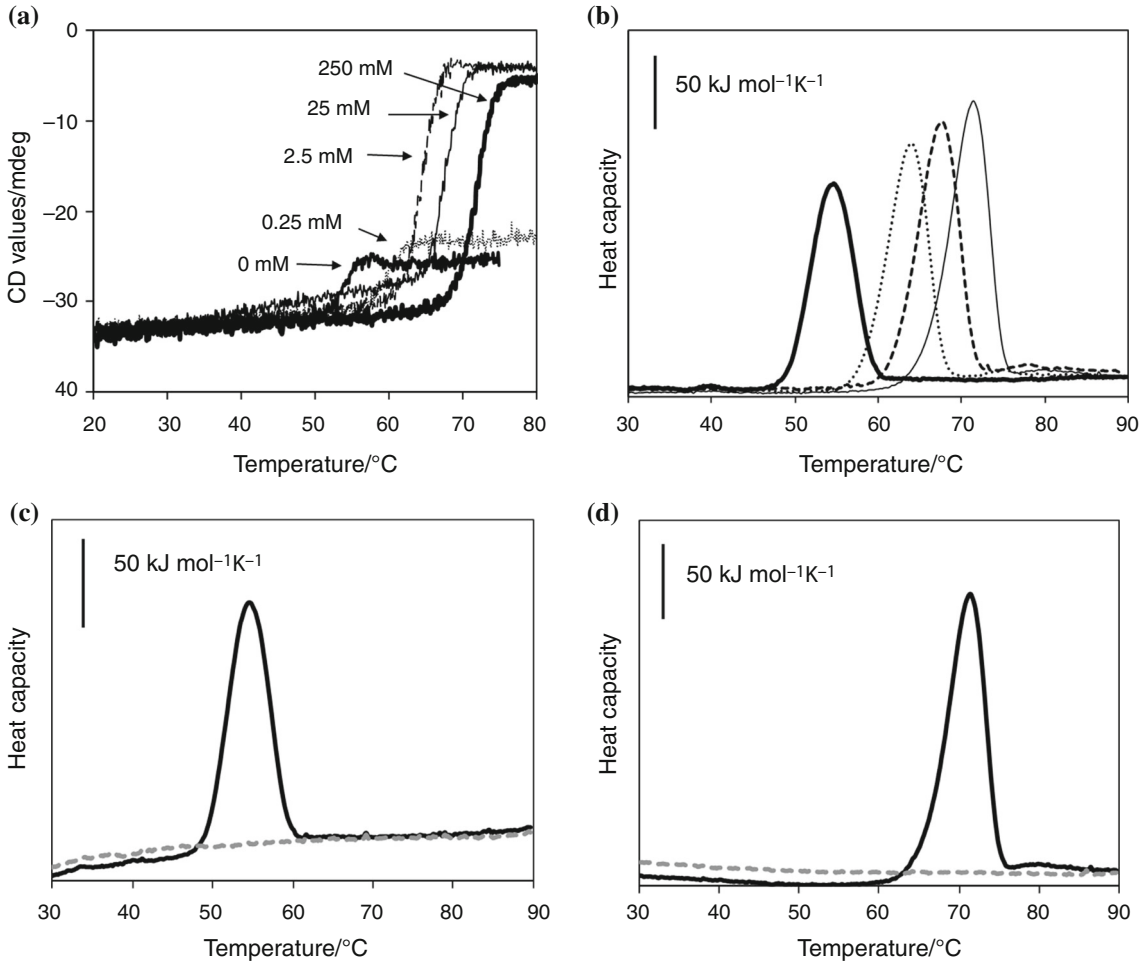

Fig. 2 Thermal stability analysis. **a** Thermal denaturation curves of Cut190*S176A under different concentrations of $CaCl_2$, obtained by monitoring the CD value at 222 nm. **b** Heat capacity curves of Cut190*S176A under different concentrations of $CaCl_2$. The solid, dotted, broken, and thin lines indicate the DSC curves under the conditions of 0, 2.5, 25, and 250 mM $CaCl_2$, respectively. **c**, **d** Heat capacity curves of Cut190*S176A at the first (solid line) and second (broken line) scans under the conditions of 0 (**c**) and 250 (**d**) mM $CaCl_2$

especially at high $CaCl_2$ concentrations. The thermal denaturation profiles at high $CaCl_2$ concentrations were different from those at low $CaCl_2$ concentrations (Fig. 2a), suggesting that Ca^{2+} binding to Cut190 could change its structural properties such as protein flexibility, which closely correlates with its function. Assuming a two-state transition, the transition temperature (T_m) and the van't Hoff enthalpy change (ΔH_{vH}) were determined by a fitting procedure (Table 1). The T_m values were almost independent of the protein concentration (0.02, 0.04, and 0.08 mg mL^{-1}, as analyzed in our CD study), while dependent on the heating rate (0.5, 1.0, and 2.0 °C min^{-1}, data not shown). A higher heating rate resulted in a higher T_m value, as is typical for irreversible thermal unfolding. Thus, the Ca^{2+}-binding effects on the thermal stability of Cut190*S176A should be comparable under the same heating rate. Similar to our previous results of Cut190 and its mutants analyzed using CD and differential scanning fluorimetry [8, 11], Ca^{2+} binding contributes to increase the stability of Cut190*S176A.

Table 1 Thermodynamic parameters for the denaturation of Cut190*S176A in the absence or presence of Ca^{2+} analyzed using CD

Ca^{2+}/mM	T_m/°C[a]	ΔT_m/°C	ΔH_{vH}/kJ mol^{-1}[a]
0	53.6 ± 0.07	0	1027 ± 65
0.25	59.6 ± 0.08	6.0	772 ± 38
2.5	64.4 ± 0.07	10.8	827 ± 11
25	67.8 ± 0.03	14.2	878 ± 13
250	71.8 ± 0.03	18.2	781 ± 10

[a]Fitting error shown

To determine the thermodynamic parameters in further detail, the thermal stabilities of Cut190*S176A under

various concentrations of $CaCl_2$ at 0, 2.5, 25, and 250 mM were analyzed using DSC (Fig. 2b). The DSC experiments showed that each heat capacity curve had a single peak and the thermal unfolding process was typically irreversible under not only high Ca^{2+} concentrations but also low Ca^{2+} concentrations (Fig. 2c, d). The DSC data were analyzed using a model of two-state transition, and the results are summarized in Table 2. Both ΔH_{cal} and ΔH_{vH} were obtained at T_d. The T_d, ΔH_{cal}, and ΔH_{vH} values of Cut190*S176A in the absence of Ca^{2+} are 54.4 °C, 861 kJ mol^{-1}, and 575 kJ mol^{-1}, respectively. The stabilities increase with increasing Ca^{2+} concentration, similar to those analyzed using CD (Table 1). The ratio of $\Delta H_{cal}/\Delta H_{vH}$ is clearly different from either 1 or 2, indicating that cooperative transition occurs.

To analyze the mechanism of increased stability of Cut190*S176A, MD simulations at 300 K were carried out on both the Ca^{2+}-bound and Ca^{2+}-free structures under various Ca^{2+} concentrations. For each system, the average fraction of native contacts, Q, with respect to their initial structure was calculated to investigate the relative stability. As shown in Fig. 3a, all of the average Q values exhibit near unity, meaning that the structures fluctuated around their initial ones. Comparing between the Ca^{2+}-bound and Ca^{2+}-free states, the values of the former are higher than those of the latter. Interestingly, the Ca^{2+}-bound structure is sensitive to the Ca^{2+} concentration, where the average Q value of the Ca^{2+}-bound structure is the lowest at 0 mM Ca^{2+} and the highest at 25 mM Ca^{2+} concentration. This result suggests that Ca^{2+} ions in the Ca^{2+} binding sites specifically act on the enzyme around 25 mM Ca^{2+} concentration. Additionally, higher Ca^{2+} concentrations result in decreasing the stability slightly, suggesting that once the Ca^{2+} binding sites have been fully saturated, additional Ca^{2+} ions start to perturb the enzyme structure. To analyze the conformational space of the Ca^{2+}-bound state, a histogram of the RMSDs of the structures at each Ca^{2+} concentration with respect to their average (30–100 ns) for each concentration is plotted in Fig. 3b. The distribution for 25 mM Ca^{2+} is the narrowest with the highest peak, and furthermore, the location of the peak along the RMSD axis is the lowest. This suggests a relatively small conformational variability in the ensemble and indicates that the protein at this concentration is the most stable. The remaining concentrations have their respective peaks at similar heights and widths, but the location of the peak along the RMSD axis varies between these concentrations. Here, 0 mM has its peak at the highest RMSD level, suggesting that at 0 mM the structures sample a wide conformational space, indicating it is the least stable system. This result is also collaborated by the PCA plots in Fig. 3c–g, where the 25 mM Ca^{2+} simulations sampled in a relatively small conformational space, while the 0 and 100 mM simulations sampled in a larger conformational space with 250 mM in between. Finally, Fig. 3h shows representative structures taken from each of the ensembles and some flexibility in the loop regions near the Ca^{2+} ions (Ser75-Gly83, Pro200-Pro213, [Glu220-His230, Asp250-Ala255, Leu286-Glu296]) can be seen, suggesting higher Ca^{2+} concentrations could interfere with the bound Ca^{2+} ions and thus disrupt protein stability.

Discussion

In this study, Ca^{2+}-dependent folding thermodynamics of Cut190*S176A were evaluated by using CD, DSC and MD simulations. Both CD and DSC results show that the stability increases with increasing $CaCl_2$ concentration. The present results of T_m values are comparable to those of Cut190 mutants with an N-terminal His-tag, reported previously [8, 11]. In order to analyze the thermodynamic origin of the stability differences, the thermodynamic parameters at 53.6 °C, the denaturation temperature of Cut190*S176A in the Ca^{2+}-free state, were calculated using the ΔC_p values at the respective conditions, as described previously [13, 14]. Within the narrow temperature range around the T_d values, the error of the calculated ΔG and ΔH values at the reference temperature should be small, even if the ΔC_p values obtained contain errors. The calculated parameters are summarized in Table 3. The increased thermal stability induced upon the Ca^{2+} binding is mainly due to the favorable ΔH, which is partially compensated by an unfavorable ΔS. The favorable ΔH could be explained by the increased contact ratios in the Ca^{2+}-bound state shown by the MD simulations. The increased contacts would result in the decreased fluctuation of Cut190*S176A in the Ca^{2+}-bound state, reflecting to the unfavorable ΔS.

Table 2 Thermodynamic parameters for the denaturation of Cut190*S176A in the absence or presence of Ca^{2+} analyzed using DSC

Ca^{2+}/mM	T_d/°C	ΔH_{cal}/kJ mol^{-1}	ΔH_{vH}/kJ mol^{-1}	$\Delta H_{cal}/\Delta H_{vH}$	ΔC_p/kJ mol^{-1} K^{-1}
0	54.4	861	575	1.50	7.48
2.5	63.5	1004	620	1.62	10.6
25	67.2	1085	624	1.74	10.8
250	71.0	1138	658	1.73	10.5

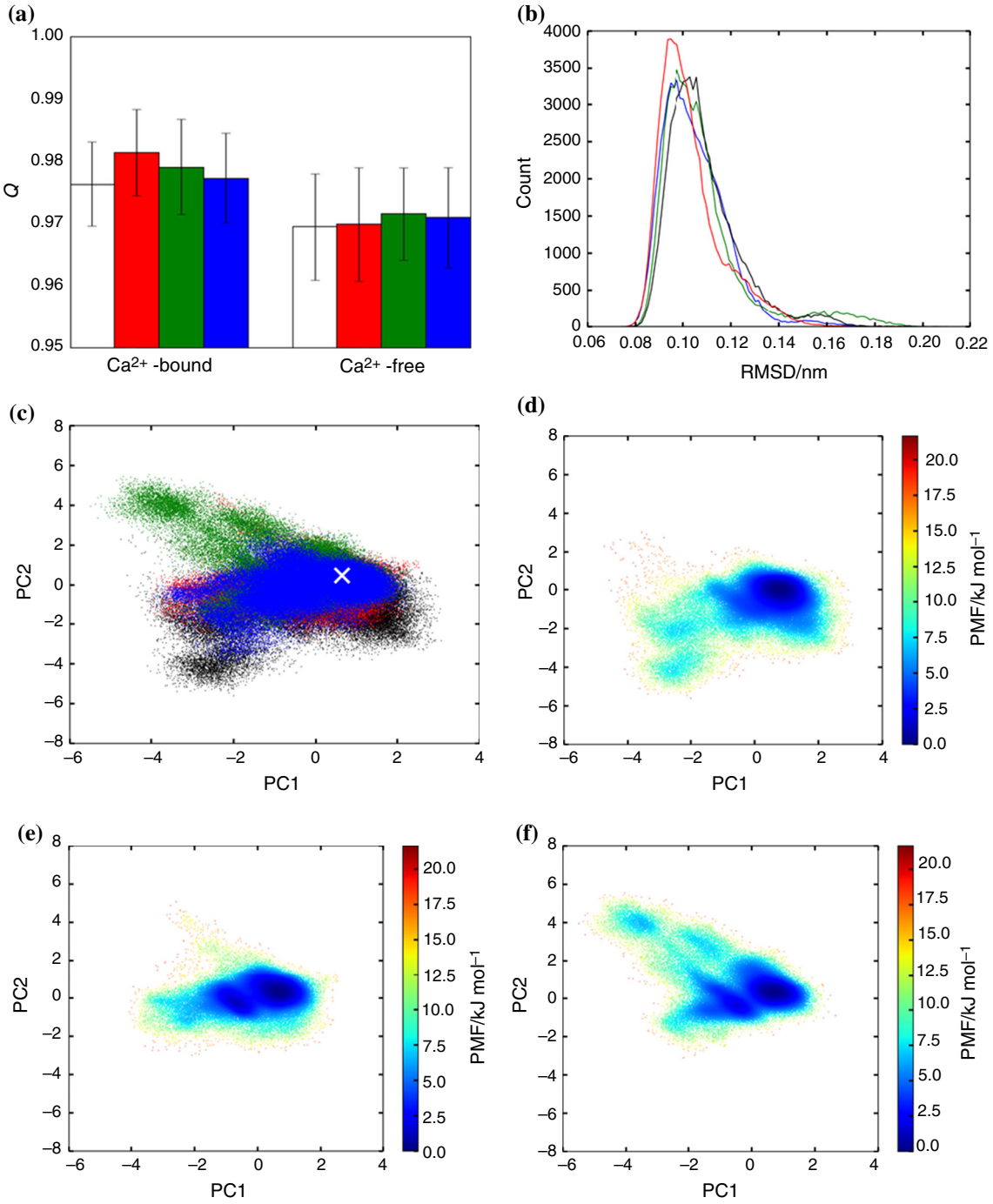

Fig. 3 Dependence of the Ca^{2+} concentration on the thermal stability obtained from the MD simulations. **a** Fraction of native contacts (Q-value) comparing the relative stability of the protein for the Ca^{2+}-bound and Ca^{2+}-free systems at four concentrations (averages with error bars), where white, red, green, and blue correspond to 0, 25, 100, and 250 mM. **b** Histogram of RMSDs of Ca^{2+}-bound structures for each concentrations against their respective average structures, where black, red, green, and blue correspond to 0, 25, 100, and 250 mM. **c** Trajectories projected onto the first principal component (PC1) and the second one (PC2) obtained from PCA of the heavy atoms of the Ca^{2+}-bound structures where black, red, green, and blue correspond to 0, 25, 100, and 250 mM, and X corresponds to the X-ray structure (Fig. 1). **d–g** Potential of mean force (PMF) for 0, 25, 100, and 250 mM, respectively, projected on to the PCA space from Fig. 3c. **h** Plot of representative structures at each concentration drawn using Molmil [32], where white, black, red, green, and blue are the X-ray, 0, 25, 100, and 250 mM structures, respectively. (Color figure online)

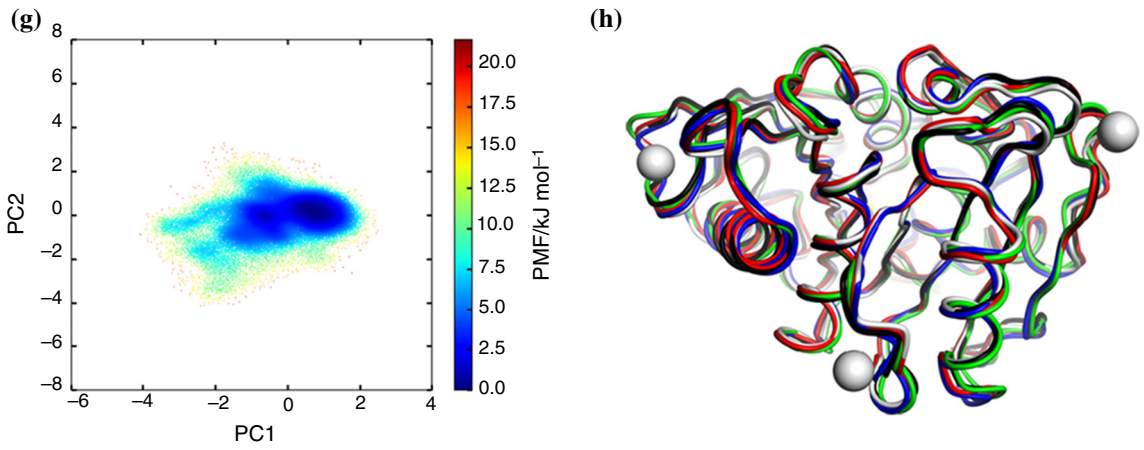

Fig. 3 continued

Table 3 Thermodynamic parameters for the denaturation of Cut190*S176A in the absence or presence of Ca^{2+} at 54.4 °C

Ca^{2+}/mM	ΔT_d/°C	$\Delta G(T)$/kJ mol^{-1}	$\Delta H(T)$/kJ mol^{-1}	$\Delta S(T)$/J mol^{-1} K^{-1}
0	0	0	861	2627
2.5	9.0	25.7	908	2693
25	12.8	37.9	947	2775
250	16.4	50.2	964	2791

Figure 4 shows a plot of ln[$CaCl_2$] versus T_m^{-1} and T_d^{-1} determined from CD and DSC, respectively. When the Ca^{2+} concentration in the free state is higher than that in the bound state, the plot corresponds to the van't Hoff analysis, whose slope provides ΔH_{vH}. As reported previously [28, 29], when the ligand concentration is much higher than the dissociation constant (K_D) for the ligand–protein interaction, the protein concentration in the bound state is much larger than that in the free state, generating a single DSC peak derived from the ligand-bound protein. Preliminary isothermal titration calorimetry experiments showed that the K_D value for Ca^{2+} binding to Cut190*S176A was in the mM order (unpublished results). The Ca^{2+} concentration range analyzed in this study was between 0.25 and 250 mM. At the lower Ca^{2+} concentrations, most of the enzymes should exist in the Ca^{2+}-free state. However, the DSC peak shifts to a higher temperature with little change in its shape, and the plot in Fig. 4 could be fitted linearly, providing ΔH_{vH} values to be 598 and 546 kJ mol^{-1}, which are comparable to those determined from CD and DSC (Tables 1 and 2). One possibility to explain this phenomena is that the association and dissociation rates of Ca^{2+} binding are so fast, mainly due to the electrostatic interaction [30, 31], that Cut190*S176A including the state close to thermal denaturation could bind to Ca^{2+}, resulting in an increased denaturation temperature by forming a transient complex.

MD simulations show that the enzyme structure does not significantly change upon different Ca^{2+} concentrations. Especially in the Ca^{2+}-free structure, no effect of the Ca^{2+} concentrations was observed. In the Ca^{2+}-bound structure, the Ca^{2+} ions perturb local regions based on the Q value, RMSD, and the PCA analyses. The mechanism is suggested as follows. In the three models with Ca^{2+} ions included (25, 100, and 250 mM), three Ca^{2+} ions are in the binding sites forming stable loop structures (Ser75-Gly83, Pro200-Pro213, [Glu220-His230, Asp250-Ala255, Leu286-Glu296]). These bound Ca^{2+} ions also interact with the surrounding environment. When the Ca^{2+} concentration is high (e.g., 250 mM), the bound ions presumably frequently interact with other Ca^{2+} ions and/or counter chloride ions. As a result, the loop structures along with the bound ions tend to fluctuate. Therefore, the Ca^{2+} concentration of 25 mM is optimal to stabilize the Ca^{2+}-bound structure. It seems to be difficult to estimate how much the Ca^{2+} concentration in the MD simulations corresponds to that in the solution in the experimental condition, because the box size of the MD system is limited. The Ca^{2+} in the MD simulations might have additional effects in solution, similar to the environments at higher Ca^{2+} concentrations. The structure transition mechanism from the Ca^{2+}-free to the Ca^{2+}-bound structures, however, remains unclear. Even at high Ca^{2+} concentrations, no conformational change in the Ca^{2+}-free structure to the

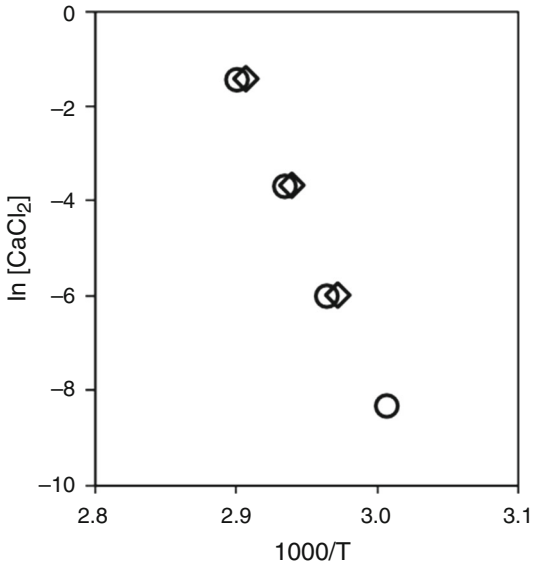

Fig. 4 Dependence of the Ca^{2+} concentration on the thermal stability. The $CaCl_2$ concentrations are plotted against T_m^{-1} from CD (◇) or T_d^{-1} from DSC (◯)

conformation of the Ca^{2+}-bound one was observed, although the Ca^{2+} ions reached equilibrium. This suggests that the Ca^{2+} ions need to bind for a considerable amount of time before the conformational change will occur. Thus, although this work has clarified the effect of Ca^{2+} ions on the Ca^{2+}-bound structure, further long MD simulations (e.g., > 1 ms) are required to show this transition, which at this point in time are unfeasible. Alternatively, enhanced sampling simulations such as multicanonical MD could be performed to speed up this process [21, 26], but such an approach is beyond the scope of this work.

Conclusions

The present MD simulations of Cut190*S176A in the absence or presence of Ca^{2+} are in good correlation with the experimental results of folding thermodynamics that Ca^{2+} binding to Cut190*S176A increases the thermal stability by increasing ΔH and decreasing ΔS, probably due to the increase in intramolecular interactions and the decrease in protein flexibility. The Ca^{2+} binding to the three sites of Cut190*S176A would change its structure into the more stable state with increasing intramolecular interactions.

Acknowledgements The authors thank Ms. Ayako Miki and Akane Senga of Kyoto Prefectural University for protein preparation, Dr. Nobutaka Numoto of Tokyo Medical and Dental University for crystal structure information, and Dr. Harumi Fukada of Osaka Prefecture University for critical reading of the manuscript. The CD and DSC experiments were performed at the Okinawa Institute Science and Technology Graduate University (OIST). This work was supported by the Research Grant from Institute for Fermentation, Osaka (IFO) to M.O. This work was also supported by Grand-in-Aid for Scientific Research C (JP16K07331) from the Japan Society for the Promotion of Science (JSPS) to N.K. It was performed in part under the Cooperative Research Program of the Institute for Protein Research, Osaka University, CR-17-05 and CR-18-02. Computational resources of a PC cluster were partly provided by the HPCI Research Project (hp150146 and hp170024).

References

1. Purdy RE, Kolattukudy PE. Hydrolysis of plant cuticle by plant pathogens. Properties of cutinase I, cutinase II, and a nonspecific esterase isolated from *Fusarium solani pisi*. Biochemistry. 1975;14:2832–40.
2. Nyyssölä A. Which properties of cutinases are important for applications? Appl Microbiol Biotechnol. 2015;99:4931–42.
3. Carvalho CM, Aires-Barros MR, Cabral JM. Cutinase: from molecular level to bioprocess development. Biotechnol Bioeng. 1999;66:17–34.
4. Bornscheuer UT. Microbial carboxyl esterases: classification, properties and applications in biocatalysis. FEMS Microbiol Rev. 2002;26:73–81.
5. Pio TF, Macedo GA. Cutinases: properties and industrial applications. Adv Appl Microbiol. 2009;66:77–95.
6. Zimmermann W, Billig S. Enzymes for the biofunctionalization of poly(ethylene terephthalate). Adv Biochem Eng Biotechnol. 2010;125:97–120.
7. Chen S, Su L, Chen J, Wu J. Cutinases: characteristics, preparation, and application. Biotechnol Adv. 2013;31:1754–67.
8. Kawai F, Oda M, Tamashiro T, Waku T, Tanaka N, Yamamoto M, Mizushima H, Miyakawa T, Tanokura M. A novel Ca^{2+}-activated, thermostabilized polyesterase capable of hydrolyzing polyethylene terephthalate from *Saccharomonospora viridis* AHK190. Appl Microbiol Biotechnol. 2014;98:10053–64.
9. Hu X, Thumarat U, Zhang X, Tang M, Kawai F. Diversity of polyester-degrading bacteria in compost and molecular analysis of a thermoactive esterase from *Thermobifida alba* AHK119. Appl Microbiol Biotechnol. 2010;87:771–9.
10. Thumarat U, Kawabata T, Nakajima M, Nakajima H, Sugiyama A, Yazaki K, Tada T, Waku T, Tanaka N, Kawai F. Comparison of genetic structures and biochemical properties of tandem cutinase-type polyesterases from *Thermobifida alba* AHK119. J Biosci Bioeng. 2015;120:491–7.
11. Miyakawa T, Mizushima H, Ohtsuka J, Oda M, Kawai F, Tanokura M. Structural basis for the Ca^{2+}-enhanced thermostability and activity of PET-degrading cutinase-like enzyme from *Saccharomonospora viridis* AHK190. Appl Microbiol Biotechnol. 2015;99:4297–307.
12. Miller JH. Experiments in molecular biology. New York: Cold Spring Harbor Laboratory; 1972. p. 431–3.
13. Inaba S, Fukada H, Ikegami T, Oda M. Thermodynamic effects of multiple protein conformations on stability and DNA binding. Arch Biochem Biophys. 2013;537:225–32.
14. Inaba S, Fukada H, Oda M. Effect of a salt-bridge between interrepeats on the 3D structure of the c-Myb DNA-binding domain revealed by thermodynamic analysis. J Therm Anal Calorim. 2018;131:335–41.
15. Lindorff-Larsen K, Piana S, Palmo K, Maragakis P, Klepeis JL, Dror RO, Shaw DE. Improved side-chain torsion potentials for the Amber ff99SB protein force field. Proteins. 2010;78:1950–8.
16. Jorgensen WL, Chandrasekhar J, Madura JD, Impey RW, Klein ML. Comparison of simple potential functions for simulating liquid water. J Chem Phys. 1983;79:926–35.

17. Joung IS, Cheatham TE 3rd. Determination of alkali and halide monovalent ion parameters for use in explicitly solvated biomolecular simulations. J Phys Chem B. 2008;112:9020–41.
18. Li P, Roberts BP, Chakravorty DK, Merz KM Jr. Rational design of particle mesh Ewald compatible Lennard-Jones parameters for +2 metal cations in explicit solvent. J Chem Theory Comput. 2013;9:2733–48.
19. Abraham MJ, Murtola T, Schulz R, Páll S, Smith JC, Hess B, Lindahl E. GROMACS: high performance molecular simulations through multi-level parallelism from laptops to supercomputers. SoftwareX. 2015;1–2:19–25.
20. Fukuda I, Kamiya N, Yonezawa Y, Nakamura H. Simple and accurate scheme to compute electrostatic interaction: zero-dipole summation technique for molecular system and application to bulk water. J Chem Phys. 2012;137:054314.
21. Bekker G-J, Kamiya N, Araki M, Fukuda I, Okuno Y, Nakamura H. Accurate prediction of complex structure and affinity for a flexible protein receptor and its inhibitor. J Chem Theory Comput. 2017;13:2389–99.
22. Essmann U, Perera L, Berkowitz ML, Darden T, Lee H, Pedersen LG. A smooth particle mesh Ewald method. J Chem Phys. 1995;103:8577–93.
23. Kamiya N, Fukuda I, Nakamura H. Application of zero-dipole summation method to molecular dynamics simulations of a membrane protein system Chem. Phys Lett. 2013;568–569:26–32.
24. Arakawa T, Kamiya N, Nakamura H, Fukuda I. Molecular dynamics simulations of double-stranded DNA in an explicit solvent model with the zero-dipole summation method. PLoS ONE. 2013;8:e76606.
25. Kamiya N, Mashimo T, Takano Y, Kon T, Kurisu G, Nakamura H. Elastic properties of dynein motor domain obtained from all-atom molecular dynamics simulations. Protein Eng Des Sel. 2016;29:317–25.
26. Nishigami H, Kamiya N, Nakamura H. Revisiting antibody modeling assessment for CDR-H3 loop. Protein Eng Des Sel. 2016;29:477–84.
27. Oda M, Inaba S, Kamiya N, Bekker G-J, Mikami B. Structural and thermodynamic characterization of endo-1,3-β-glucanase: insights into the substrate recognition mechanism. Biochim Biophys Acta. 2018;1866:415–25.
28. Fukada H, Sturtevant JM, Quiocho FA. Thermodynamics of the binding of L-arabinose and of D-galactose to the L-arabinose-binding protein of *Escherichia coli*. J Biol Chem. 1983;258:13193–8.
29. Sturtevant JM. Biochemical applications of differential scanning calorimetry. Ann Rev Phys Chem. 1987;38:463–88.
30. Wade RC, Gabdoulline RR, Lüdemann SK, Lounnas V. Proc Natl Acad Sci USA. 1998;95:5942–9.
31. Oda M, Nakamura H. Thermodynamic and kinetic analyses for understanding sequence-specific DNA recognition. Genes Cells. 2000;5:319–26.
32. Bekker G-J, Nakamura H, Kinjo AR. Molmil: a molecular viewer for the PDB and beyond. J Cheminform. 2016;8:42.